Crystal chemistry of poppiite, V-analogue of pumpellyite, from the Komatsu mine, Saitama Prefecture, Japan

Mariko NAGASHIMA*, Takashi MATSUMOTO**, Takashi YAMADA***, Minoru TAKIZAWA*** and Koichi MOMMA†

*Graduate School of Sciences and Technology for Innovation, Yamaguchi University, Yamaguchi 753–8512, Japan
**Application Laboratories, Rigaku Corporation, Akishima, Tokyo 196–8666, Japan
***Friends of Mineral, Tokyo, Toyotamanaka 4–13–18, Nerima, Tokyo 176–0013, Japan
†National Museum of Nature and Science, Tsukuba, Ibaraki 305–0005, Japan

The crystal chemistry of poppiite, V-analogue of pumpellyite-group mineral, from the Komatsu mine, Saitama Prefecture, Japan and from the Gambatesa mine, Genova, Italy (type locality) were studied using electron microprobe (EMPA) and X-ray single-crystal diffraction methods. Both samples are characterized by very high V content, and the average V_2O_3 content is 31.1 wt% for the Komatsu poppiite and 25.4 wt% for the Gambatesa specimen. The Komatsu specimen in this study is the V-richest poppiite ever reported. Structure refinements converged to R_1 values of 5.01% for Komatsu and 3.74% for Gambatesa. The determined structural formula (Z = 4) of poppiite from the Komatsu and Gambatesa mines is $Ca_{2.00}{}^{X}(V^{3+}_{0.54}Fe^{3+}_{0.01}Mg_{0.19}Mn^{2+}_{0.22}Al_{0.04})^{Y}(V^{3+}_{1.73}Fe^{3+}_{0.03}Al_{0.24})Si_{3.00}O_{10.59}(OH)_{3.41}$, and $Ca_{2.00}{}^{X}(V^{3+}_{0.49}Fe^{3+}_{0.08}Mg_{0.19}Mn^{2+}_{0.17}Al_{0.07})^{Y}(V^{3+}_{1.35}Fe^{3+}_{0.21}Al_{0.44})Si_{3.00}O_{10.64}(OH)_{3.36}$, respectively. Both specimens are classified as poppiite-(V^{3+}) because the X and Y octahedral sites are predominantly occupied by V^{3+}. The Me^{2+}:Me^{3+} ratio at X in this study is 0.41:0.59 for the Komatsu poppiite, and 0.36:0.64 for the Gambatesa one. The former has the larger unit-cell volume (1033.2 Å^3) than the latter (1026.6 Å^3). Both charge distribution analysis and located hydrogen sites indicate that O5, O7, O10, and O11 positions host hydroxyl groups. The <Y-O> distance and cell-dimensions positively correlate with mean ionic radius at Y. On the other hand, the ***a***- and ***c***-dimensions are shorter than the values expected by the regression lines estimated by approximately Me^{2+}:$Me^{3+} \approx 0.5$: 0.5 because of the high proportion of Me^{3+} at X. The studied poppiite crystals are characterized by small β angles [97.283(2)° for Komatsu, and 97.343(3)° for Gambatesa]. These values are considered to be related to distortional variations of the YO_6 octahedra caused by the different characteristics of octahedral V^{3+} ions compared to Fe^{3+} and Cr^{3+}.

Keywords: Poppiite, V^{3+}, Pumpellyite, Crystal structure

INTRODUCTION

Pumpellyite-group minerals are formed under low-grade metamorphic conditions and at low-temperature hydrothermal activity (e.g., Deer et al., 1986). Because the pumpellyite-group minerals are rather complex both compositionally and structurally, their crystal chemistry is not well understood. The structure of pumpellyite is monoclinic of space group $A2/m$ (standard setting $C2/m$). The pumpellyite structure consists of isolated [SiO_4] tetrahedra and disilicate [Si_2O_6(OH)] groups. The tetrahedral units connect two symmetrically independent edge-sharing chains of X and Y octahedra, running along the ***b***-axis (Gottardi, 1965). The general formula is $^{VII}W_2{}^{VI}X^{VI}Y_2{}^{IV}Z_3O_{14-n}(OH)_n$ with $4 \geq n \geq 3$ (Z = 4, Passaglia and Gottardi, 1973). The W site is subdivided into W1 and W2, both occupied by Ca. The Z sites, Z1–3, are occupied by Si. In general, both divalent (Me^{2+}) and trivalent (Me^{3+}) cations, such as Mg, Al, Fe^{2+}, Fe^{3+}, Mn^{2+}, Mn^{3+}, V^{3+}, and Cr^{3+}, occupy X whereas Y is occupied by Me^{3+} only. Pumpellyite-group minerals are named after the predominant cation at Y, and they are further distinguished by a suffix that denotes the cation which predominates at X (Passaglia and Gottardi, 1973). The poppiite, $^{Y}V^{3+}$-analogue of the pumpellyite-group mineral, was defined by Brigatti et al. (2006) from the Gambatesa mine, Genova, Italy. The obtained structural formula in their study was $^{W}(Ca_{1.92}Na_{0.07}K_{0.01}Rb_{0.01})_{\Sigma 2.01}{}^{X}(V^{3+}_{0.32}Fe^{3+}_{0.26}Mg_{0.20}Mn^{2+}_{0.15}Al_{0.08}Cu^{2+}_{0.01})_{\Sigma 1.02}{}^{Y}(V^{3+}_{1.72}Al_{0.26}Ti_{0.01})_{\Sigma 1.99}{}^{Z}(Si_{2.92}Al_{0.08})O_{14}(OH)_{3.5}$. V^{3+}-rich

doi:10.2465/jmps.180613
N. Nagashima, nagashim@yamaguchi-u.ac.jp Corresponding author

pumpellyite from the Hemlo gold deposit, Ontario, Canada, with ~ 1.85 V^{3+} atoms per formula unit (apfu), probably corresponding to poppiite, was described by Pan and Fleet (1992a, 1992b). A third occurrence was recently reported from the Komatsu mine, Saitama Prefecture, Japan (Yamada et al., 2014). In our preliminary study, the Komatsu poppiite was richer in V_2O_3 than the others. Here, we report the crystal structure of poppiite from the Komatsu mine in order to demonstrate the relationship between the V distribution and structural variation. For comparison, a poppiite specimen from the Gambatesa mine (type locality) is also re-examined. This is the second report of X-ray single-crystal structure refinements of poppiite.

SAMPLES

The Komatsu mine is a metasedimentary manganese deposit. Aggregates of fibrous poppiite associated with Mn-bearing calcite, goldmanite $Ca_3V_2^{3+}(SiO_4)_3$, V-bearing axinite-(Mn) $Ca_4Mn_2^{2+}Al_4[B_2Si_8O_{30}](OH)_2$, rhodonite $Mn^{2+}SiO_3$, and djurleite like Cu-S mineral were found at the dump of this mine (Yamada et al., 2014). The poppiite crystals are deep green in color. From this mine, some vanadium-rich minerals, such as ansermetite ($Mn^{2+}V_2^{5+}O_6{\cdot}4H_2O$), fianelite ($Mn_2^{2+}V_2O_7{\cdot}2H_2O$), franciscanite [$Mn_6^{2+}V^{5+}(SiO_4)_2(O,OH)_6$], and vuorelainenite ($Mn^{2+}V_2^{3+}O_4$) are observed (Yamada and Takizawa, 2007; Yamada et al., 2014). Hausmannite, rhodonite, caryopilite, jacobsite, and rhodochrosite also occur in the ores from this mine. The studied Komatsu poppiite is deposited in the National Museum of Nature and Science, Tokyo, Japan (NSM-M46018).

In our specimen, the poppiite from the Gambatesa mine (type loc.) is closely associated with goldmanite. Prismatic platy crystals up to 0.5 mm long are assembled to aggregates of dark brown color. Details of the occurrence were reported by Brigatti et al. (2006).

EXPERIMENTAL METHODS

The chemical compositions were determined using a JEOL JXA-8230 electron microprobe analyzer (EMPA) at the Centre for Instrumental Analysis, Yamaguchi University, Japan. Operating conditions were: accelerating voltage of 15 kV, a beam current of 20 nA, and a beam diameter of 1 μm. Wavelength-dispersion spectra were collected with LiF, PET, and TAP monochromator crystals to identify interfering elements and locate the best wavelengths for background measurements. The abundances of Si, Ti, Al, Cr, V, Fe, Mn, Mg, Ca, Sr, Ba, Na, K, Ni, Cu, Zn, P, F, and Cl were measured. Several elements, which are not listed in Table 1, are below the detection limit. The ZAF method was used for data correction.

Table 1. Chemical compositions of poppiite samples

	The Komatsu mine, Saitama, Japan		The Gambatesa mine, Genova, Italy	
	Ave.	Range	Ave.	Range
	n = 6		n = 6	
SiO_2	33.10	33.00-33.21	33.51	33.31-33.86
TiO_2	0.03	0.00-0.10	0.11	0.08-0.17
Al_2O_3	2.61	2.07-3.31	4.88	4.04-5.52
V_2O_3*	31.14	30.03-32.08	25.35	24.52-27.61
Fe_2O_3*	0.64	0.43-0.97	4.13	3.50-4.84
MnO*	2.83	2.08-3.43	2.18	2.10-2.31
NiO	0.01	0.00-0.05	0.03	0.00-0.06
MgO	1.38	0.81-1.93	1.41	0.83-1.83
CaO	20.47	20.27-20.67	20.85	20.67-20.97
BaO	0.01	0.00-0.07	0.01	0.00-0.06
Na_2O	0.07	0.04-0.08	0.11	0.03-0.18
K_2O	0.01	0.00-0.03	0.01	0.00-0.01
H_2O (calc.)	5.68		5.65	
Total	97.99		98.25	
Σcations = 8				
Si	3.00	2.97-3.02	3.00	2.98-3.01
Ti	0.00	0.00-0.01	0.01	0.01
Al	0.28	0.22-0.35	0.51	0.43-0.58
V	2.27	2.19-2.34	1.82	1.76-1.99
Fe	0.04	0.03-0.07	0.28	0.23-0.33
Mn	0.22	0.16-0.27	0.17	0.16-0.18
Ni	0.00	0.00	0.00	0.00
Mg	0.19	0.11-0.26	0.19	0.11-0.24
Ca	1.99	1.98-2.00	2.00	1.99-2.02
Ba	0.00	0.00	0.00	0.00
Na	0.01	0.00-0.01	0.02	0.01-0.03
K	0.00	0.00	0.00	0.00
Total	8.00		8.00	

* V as V_2O_3, Fe as Fe_2O_3 and Mn as MnO.

At first, Komatsu poppiite was measured using Mo$K\alpha$ radiation, but because it was an aggregate of several crystals, most diffraction spots were overlapped and the quality of data was significantly low. Therefore, in order to improve the separation of diffraction spots, we measured this Komatsu poppiite using Cu$K\alpha$ radiation. As a result, the quality of the data has been improved. The diffraction data of Komatsu poppiite (0.04 × 0.02 × 0.02 mm) was collected at room temperature on a Rigaku FR-X Cu$K\alpha$ (λ = 1.54184 Å) rotating anode generator equipped with VariMax optics, an AFC12 goniometer and HyPix-6000HE detector at Rigaku Corporation, Japan. Preliminary lattice parameters and an orientation matrix were obtained from six sets of frames and refined during the integration process of the intensity data. The diffraction data were processed using CrysAlisPro (Ri-

gaku oxford diffraction, 2018). An empirical absorption correction using CrysAlisPro (Rigaku oxford diffraction, 2018) was applied.

The diffraction data of Gambatesa poppiite (0.10 × 0.04 × 0.01 mm) was collected at room temperature with graphite-monochromated Mo$K\alpha$ X-radiation (λ = 0.71073 Å) using a Bruker SMART APEX II CCD diffractometer installed at Shimane University, Japan. Preliminary lattice parameters and an orientation matrix were obtained from three sets of frames and refined during the integration process of the intensity data. Diffraction data were collected with ω scans with different φ settings (φ-ω scan) (Bruker, 1999). Data were processed using SAINT (Bruker, 1999). An empirical absorption correction using SADABS (Sheldrick, 1996) was applied.

For both samples, structural refinements were performed using the program SHELXL-97 (Sheldrick, 2008). Scattering factors for neutral atoms were employed. At the primary stage populations of Ca at W1 and W2, and Si at Z1, Z2, and Z3 were refined. However, these sites turned out to be fully occupied within one standard deviation. Thus, the site occupancies at these sites were fixed at 1.0. The site occupancies of X and Y were refined with V versus Mg, and V versus Al, respectively. X-ray data cannot discriminate between Al and Mg due to similar scattering factors. Thus, the Al content may also cover Mg and vice versa. Positions of the hydrogen atoms of the hydroxyl groups were derived from difference-Fourier syntheses and were refined assuming half occupancy with fixed U^{iso} = 0.05 Å^2. In addition, a bond-distance constraint of O-H = 0.98(2) Å (Franks, 1973) was applied.

In order to validate the refined structures, the charge distribution (CD) analysis was applied following Nespolo et al. (1999, 2001) and Nespolo (2016). The method exploits the experimental bond distances to compute a non-integer coordination number (effective coordination number, ECoN: Hoppe, 1979), and distributes the formal oxidation number, q, of each atom among all its bonds as a function of ECoN. By labelling the computed charges with Q, the q/Q ratio for the cations is the internal criterion for such evaluation (Nespolo et al., 1999, 2001; Nespolo, 2016). $Q(ij)$ and $Q(rs)$ are the charge of PC(ij) and V(rs), respectively, computed as the result of the distribution of $q(ij)$ and $q(rs)$ based on the CHARDI algorithm, where i and r identify the atomic site, j and s the crystallographic type. PC(ij) represents an atom inside a coordination polyhedron, PC, of the ith chemical species and the jth crystallographic type, V(rs) an atom at the corner (vertex) of a coordination polyhedron, of the rth chemical species and the sth crystallographic type. The σ (%) represents the mean absolute percentage deviation of the computed charges Q with respect to the formal oxidation number q.

RESULTS

Chemical composition of poppiite

Table 1 shows the chemical compositions of poppiite from the Komatsu mine, Japan and the Gambatesa mine, Italy. The sum of cations was normalized to 8. Both samples are characterized by very high V content, and the average V_2O_3 content is 31.1 wt% (number of analytical points, n = 6) for Komatsu poppiite and 25.4 wt% (n = 6) for the Gambatesa specimen. The Komatsu poppiite hardly contains Fe_2O_3 (<1 wt%). The chemical formulae (Z = 4) of Komatsu and Gambatesa poppiites can be written as $(Ca_{1.99}Na_{0.01})_{\Sigma 2.00}(V^{3+}_{2.27}Mn_{0.22}Mg_{0.19}Al_{0.28}Fe_{0.04})_{\Sigma 3.00}Si_{3.00}O_{14-n}(OH)_n$ and $(Ca_{2.00}Na_{0.02})_{\Sigma 2.02}(V^{3+}_{1.82}Fe_{0.28}Mn_{0.17}Mg_{0.19}Al_{0.51}Ti_{0.01})_{\Sigma 2.98}Si_{3.00}O_{14-n}(OH)_n$, respectively, with n as variable depending on the oxidation state of Fe and Mn. The oxidation state of Mn and Fe in Komatsu poppiite is assumed to be divalent and trivalent, respectively on a basis of the mineral assemblages. After Brigatti et al. (2006) all Fe in Gambatesa poppiite was also considered to be trivalent, and Mn to be divalent. In this case, the numbers of OH, n, are estimated as 3.42 for Komatsu poppiite and 3.39 for Gambatesa specimen. The V_2O_3 content of the Komatsu poppiite attains up to 32.1 wt%, corresponding to 2.34 V^{3+} apfu, in this study. The Komatsu poppiite is the V-richest specimen ever reported (~ 28.9 wt% from the Gambatesa mine by Brigatti et al., 2006; ~ 25.7 wt% from the Hemlo Gold deposit by Pan and Fleet, 1992a, 1992b). The V_2O_3 content of our Gambatesa poppiite is slightly lower than that reported by Brigatti et al. (2006), but the Al_2O_3 content is higher instead, suggesting the $V^{3+} \leftrightarrow$ Al substitution. Although small amount of Rb and Cu was detected for Gambatesa poppiite by Brigatti et al. (2006), they were below detection limit in this study.

Crystal-structure refinement: site occupancy and hydrogen positions

Crystallographic data and refinement parameters of poppiite are summarized in Table 2. Structure refinements of Komatsu and Gambatesa poppiites converged at R_1 values of 5.01 and 3.74%, respectively. The refined atomic positions and anisotropic displacement parameters are listed in Tables 3 and 4. Selected interatomic distances and angles, and the volume and calculated distortion parameters of octahedral sites are listed in Table 5. The crystal structure of poppiite is shown in Figure 1.

The refined site occupancies at X and Y in Komatsu

Table 2. Experimental details of the single-crystal X-ray diffraction analysis of poppiite crystals

Sample		Komatsu	Gambatesa
Crystal size (mm)		0.02 × 0.02 × 0.04	0.01 × 0.04 × 0.10
Space group		*A* 2/*m*	
Unit-cell dimensions	*a* (Å)	8.8931(2)	8.8782(3)
	b (Å)	6.0617(1)	6.0428(2)
	c (Å)	19.3222(4)	19.2938(7)
	β (°)	97.283(2)	97.343(3)
	V (Å^3)	1033.20(3)	1026.61(4)
D_{calc} (g/cm^3)		3.41	3.40
Radiation		Cu*K*α (λ = 1.54184 Å)	Mo*K*α (λ = 0.71073 Å)
Monochromator		VariMax optics	Graphite
Diffractometer		RIGAKU HyPix-6000HE	Bruker APEXII CCD
Scan type		ω scan	φ–ω scan (Bruker, 1999)
Absorption correction		CrysAlisPro (Rigaku Oxford Diffraction, 2018)	SADABS (Sheldrick, 1996)
θ_{min}(°)		4.6	2.1
θ_{max}(°)		74.3	28.7
μ (mm^{-1})		32.12	3.59
Collected reflections		6903	13019
Unique reflctions		1150	1448
R_{int} (%)		5.08	6.29
R_σ (%)		3.74	4.03
Index ranges		-10≤*h*≤11, -7≤*k*≤7, -24≤*l*≤23	-11≤*h*≤11, -8≤*k*≤8, -25≤*l*≤26
Refinement on F^2 using		SHELXL-97 (Sheldrick, 2008)	
R_1 (%)		5.01	3.74
wR_2 (%)		13.50	8.36
Goodness of fit, *S*		1.05	1.06
No. of parameters		131	133
Weighting scheme*		$w = 1/[\sigma^2(F_o^2) + (0.1049P)^2]$	$w = 1/[\sigma^2(F_o^2) + (0.0267P)^2 + 9.44P]$
$\Delta\rho_{max}$ (e Å^{-3})		1.30 at 0.77 Å from O8	0.90 at 0.77 Å from W2
$\Delta\rho_{min}$ (e Å^{-3})		-0.96 at 0.75 Å from W1	-0.96 at 1.54 Å from O8

* The function of the weighting scheme is $w = 1/[\sigma^2(F_o^2) + (a\cdot P)^2 + b\cdot P]$, where $P = [\mathrm{Max}(F_o^2) + 2F_c^2]/3$, and the parameters *a* and *b* are chosen to minimize the differences in the variances for reflections in different ranges of intensity and diffraction angle.

poppiite were $V_{0.855(16)}Mg_{0.145}$ and $V_{0.882(14)}Al_{0.118}$, respectively (Table 3). The total V content in the final refinement was ~ 2.62(2) apfu (= 0.855 + 0.882 × 2) which is close to sum of V, Fe, and Mn content, 2.53(7) apfu, derived from EMPA (Table 1). The refined site occupancies at X and Y in Gambatesa poppiite are $V_{0.756(10)}Mg_{0.244}$ and $Fe_{0.780(8)}Al_{0.220}$, respectively (Table 3), summing up (0.756 + 0.780 × 2) to ~ 2.32(1) V apfu. This value is consistent with Σ(V + Fe + Mn), 2.27(9) apfu, of the EMPA data within standard deviation (Table 1).

The determined hydrogen positions were fixed at half occupancy, and are listed in Table 3. The oxygen atoms at O5, O7, O10, and O11 positions behave as donor of a hydrogen bond, which is consistent with previous studies (e.g., Allmann and Donnay, 1971, 1973; Yoshiasa and Matsumoto, 1985; Brigatti et al., 2006; Nagashima et al., 2006; Nagashima and Akasaka, 2007; Nagashima et al., 2010). In Komatsu poppiite, the hydrogen positions at H5B, H7, H10, and H11 were determined whereas a more disordered distribution at H5A, H5B, H7, H10, and H11 was observed for Gambatesa poppiite. Tables 6 and 7 show the results by the CD analysis using the CHARDI-2015 program (Nespolo, 2016). The calculated ECoN(*ij*) for cation sites is listed in Table 6. The ECoN(*ij*) of the W sites is 6.78-6.85 for W1 and 6.15-6.18 for W2. The W1 polyhedra is represented as 7-coordinated whereas W2 has (6 + 1) coordination (Table 5). Relative large σ values obtained for the Komatsu specimen (7.1% for the center atom and 4.9% for the vertex of coordination polyhedra in Table 6) are obviously due to the undetermined hydrogen positions. As the results of structural study of julgoldite, the hydrogen positions at H5A, H7A, H7B, H10, and H11 were observed (Nagashima et al., 2018). Because the position of H7 determined in this study corresponds to that of H7B in the julgoldite, it hereafter refers to H7B.

Table 3. Atomic positions and equivalent displacement parameters (Å^2)* and occupancies of poppiite samples

Site	W**	Komatsu					Gambatesa				
		Occupancy	*x*	*y*	*z*	U^{eq}	Occupancy	*x*	*y*	*z*	U^{eq}
W1	4*i*	$Ca_{1.0}$	0.25338(15)	½	0.33996(7)	0.0229(4)	$Ca_{1.0}$	0.25295(14)	½	0.33958(6)	0.0111(3)
W2	4*i*	$Ca_{1.0}$	0.19255(16)	½	0.15605(7)	0.0235(4)	$Ca_{1.0}$	0.19290(15)	½	0.15588(7)	0.0136(3)
X	4*f*	$V_{0.855(16)}Mg_{0.145}$	½	¼	¼	0.0177(5)	$V_{0.756(10)}Mg_{0.244}$	½	¼	¼	0.0076(3)
Y	8*j*	$V_{0.882(14)}Al_{0.118}$	0.25308(8)	0.24827(12)	0.49534(4)	0.0158(4)	$V_{0.780(8)}Al_{0.220}$	0.25344(8)	0.24762(13)	0.49547(4)	0.0061(2)
Z1	4*i*	$Si_{1.0}$	0.05134(18)	0	0.09406(9)	0.0168(4)	$Si_{1.0}$	0.05090(17)	0	0.09342(8)	0.0076(3)
Z2	4*i*	$Si_{1.0}$	0.16430(18)	0	0.24898(9)	0.0186(4)	$Si_{1.0}$	0.16307(18)	0	0.24868(8)	0.0087(3)
Z3	4*i*	$Si_{1.0}$	0.46561(18)	0	0.40215(9)	0.0166(4)	$Si_{1.0}$	0.46493(17)	0	0.40171(8)	0.0076(3)
O1	8*j*		0.1382(4)	0.2215(6)	0.07632(17)	0.0197(7)		0.1379(3)	0.2218(5)	0.07548(14)	0.0113(6)
O2	8*j*		0.2635(4)	0.2269(6)	0.24699(17)	0.0218(8)		0.2616(3)	0.2279(5)	0.24702(14)	0.0111(6)
O3	8*j*		0.3652(4)	0.2190(6)	0.41332(17)	0.0195(7)		0.3654(3)	0.2187(5)	0.41435(14)	0.0106(6)
O4	4*i*		0.1250(5)	½	0.4416(2)	0.0189(9)		0.1266(4)	½	0.4427(2)	0.0086(8)
O5	4*i*		0.1238(5)	0	0.4578(2)	0.0205(9)		0.1242(5)	0	0.4578(2)	0.0123(9)
O6	4*i*		0.3749(5)	½	0.0459(2)	0.0188(9)		0.3734(4)	½	0.0458(2)	0.0093(8)
O7	4*i*		0.3768(5)	0	0.0330(3)	0.0207(10)		0.3761(4)	0	0.0335(2)	0.0123(9)
O8	4*i*		0.0349(5)	0	0.1787(2)	0.0211(10)		0.0331(4)	0	0.1780(2)	0.0100(8)
O9	4*i*		0.4735(5)	½	0.1758(2)	0.0201(10)		0.5245(5)	½	0.3244(2)	0.0121(9)
O10	4*i*		0.0645(5)	0	0.3143(3)	0.0246(10)		0.0642(5)	0	0.3144(2)	0.0147(9)
O11	4*i*		0.5014(5)	½	0.3154(3)	0.0224(10)		0.5030(5)	½	0.3161(2)	0.0113(9)
H5A	4*i*						$H_{0.5}$	0.020(7)	0	0.469(9)	0.05
H5B	4*i*	$H_{0.5}$	0.08(2)	0	0.408(3)	0.05	$H_{0.5}$	0.13(2)	0	0.408(2)	0.05
H7	4*i*	$H_{0.5}$	0.40(3)	0	0.0838(15)	0.05	$H_{0.5}$	0.464(13)	0	0.070(7)	0.05
H10	4*i*	$H_{0.5}$	0.151(16)	0	0.351(8)	0.05	$H_{0.5}$	0.139(15)	0	0.356(5)	0.05
H11	4*i*	$H_{0.5}$	0.50(3)	½	0.366(2)	0.05	$H_{0.5}$	0.592(12)	½	0.352(7)	0.05

* Thermal parameter for H atoms was fixed as 0.05 U^{iso}.

** *W*, Wyckoff notation of point position.

Table 4. Anisotropic displacement parameters (Å^2)

Site	U^{11}	U^{22}	U^{33}	U^{23}	U^{13}	U^{12}
			Komatsu			
W1	0.0216(7)	0.0234(8)	0.0248(7)	0	0.0076(5)	0
W2	0.0278(7)	0.0184(7)	0.0239(7)	0	0.0017(5)	0
X	0.0136(7)	0.0174(7)	0.0228(8)	0.0008(4)	0.0047(5)	0.0002(4)
Y	0.0124(5)	0.0155(6)	0.0197(5)	-0.0002(3)	0.0034(3)	-0.0002(3)
Z1	0.0129(7)	0.0172(9)	0.0206(9)	0	0.0034(6)	0
Z2	0.0149(8)	0.0177(8)	0.0226(9)	0	0.0005(6)	0
Z3	0.0137(7)	0.0168(9)	0.0197(9)	0	0.0038(6)	0
O1	0.0188(16)	0.0164(16)	0.0248(17)	-0.0005(12)	0.0065(13)	-0.0018(11)
O2	0.0184(16)	0.0188(17)	0.0278(19)	-0.0003(13)	0.0014(13)	-0.0009(11)
O3	0.0174(15)	0.0189(16)	0.0231(16)	0.0004(12)	0.0060(12)	0.0011(11)
O4	0.016(2)	0.015(2)	0.025(2)	0	0.0027(16)	0
O5	0.018(2)	0.019(2)	0.025(2)	0	0.0014(17)	0
O6	0.016(2)	0.015(2)	0.025(2)	0	0.0028(17)	0
O7	0.016(2)	0.016(2)	0.030(2)	0	0.0050(17)	0
O8	0.019(2)	0.022(2)	0.023(2)	0	0.0019(17)	0
O9	0.019(2)	0.019(2)	0.022(2)	0	0.0047(17)	0
O10	0.019(2)	0.030(3)	0.026(2)	0	0.0045(18)	0
O11	0.019(2)	0.020(2)	0.029(2)	0	0.0081(18)	0
			Gambatesa			
W1	0.0136(6)	0.0115(6)	0.0085(6)	0	0.0023(4)	0
W2	0.0234(6)	0.0085(6)	0.0081(6)	0	-0.0007(5)	0
X	0.0098(5)	0.0064(5)	0.0069(6)	0.0005(4)	0.0020(4)	0.0002(4)
Y	0.0076(4)	0.0063(4)	0.0044(4)	0.0003(3)	0.0013(2)	0.0004(3)
Z1	0.0080(7)	0.0091(7)	0.0054(8)	0	-0.0007(6)	0
Z2	0.0111(7)	0.0070(7)	0.0074(8)	0	-0.0009(6)	0
Z3	0.0079(7)	0.0089(7)	0.0058(8)	0	0.0008(6)	0
O1	0.0141(14)	0.0108(14)	0.0098(14)	-0.0007(12)	0.0047(11)	-0.0019(12)
O2	0.0127(13)	0.0096(13)	0.0101(14)	-0.0011(12)	-0.0020(10)	-0.0004(11)
O3	0.0144(14)	0.0106(14)	0.0075(13)	0.0027(11)	0.0040(11)	0.0008(11)
O4	0.0115(19)	0.0097(19)	0.0040(19)	0	-0.0009(15)	0
O5	0.012(2)	0.013(2)	0.012(2)	0	0.0011(17)	0
O6	0.0111(19)	0.0081(19)	0.008(2)	0	-0.0011(15)	0
O7	0.010(2)	0.012(2)	0.015(2)	0	0.0001(17)	0
O8	0.0087(19)	0.013(2)	0.008(2)	0	-0.0004(15)	0
O9	0.013(2)	0.019(2)	0.005(2)	0	0.0016(15)	0
O10	0.014(2)	0.021(2)	0.009(2)	0	0.0009(17)	0
O11	0.013(2)	0.014(2)	0.006(2)	0	0.0005(16)	0

DISCUSSION

Cation distribution at X and Y of poppiite

Determination of the site occupancies at X and Y sites in pumpellyite-group minerals is not straightforward. As mentioned above, the refined site occupancies at X and Y were $^{X}(V_{0.86(2)}Mg_{0.14})^{Y}(V_{0.88(1)}Al_{0.12})$ in Komatsu specimen (numbers of electron, Nos. e^- = 21.46 for X and 43.60 for 2Y), and $^{X}(V_{0.76(1)}Mg_{0.24})^{Y}(Fe_{0.780(8)}Al_{0.220})$ for the Gambatesa one (Nos. e^- = 20.36 for X and 41.60 for 2Y) (Table 3). However, the refined V content at X and Y covers Mn and Fe contents, and the refined Mg at X covers Al content. Measured average Al, Mg, Fe^{3+}, and Mn^{2+} contents (EMPA) were 0.28, 0.19, 0.04, and 0.22 for Komatsu poppiite, and 0.51, 0.19, 0.28, and 0.17 for the Gambatesa specimen. Divalent octahedral cations, Mg and Mn^{2+}, locate at X, whereas trivalent Fe^{3+} and Al^{3+} ions spread over both X and Y. The Al occupancy of X was estimated as follows; Al at X = (total Al content by EMPA) − 2 × (the refined site occupancy of Al at Y). Moreover, on the basis of similar ionic radii of V^{3+} (0.64 Å: Shannon 1976) and Fe^{3+} (0.645 Å), their behavior is assumed to be similar. Thus, in this study, the site occupancies of V^{3+} and Fe^{3+} at X and Y are determined based on their proportional ratios. The Fe/(V + Fe) ratio is 0.017 [= 0.04/(2.27 + 0.04)] for the Komatsu specimen, and 0.133 [= 0.28/(1.82 + 0.28)] for the Gambatesa one. Consequently, the

Table 5. Selected interatomic distances (Å) and angle (°), and volume (Å^3) and distortion parameters of the octahedral sites*

		Komatsu	Gambatesa			Komatsu	Gambatesa
W1–O2	×2	2.453(4)	2.436(3)	Z1–O1	×2	1.608(3)	1.607(3)
–O3	×2	2.354(3)	2.366(3)	–O4		1.631(5)	1.640(4)
–O4		2.393(5)	2.406(4)	–O8		1.660(5)	1.659(4)
–O8		2.544(5)	2.519(4)		Mean	1.627	1.628
–O11		2.315(4)	2.321(4)				
	Mean	2.410	2.407	Z2–O2	×2	1.637(4)	1.634(3)
				–O8		1.665(5)	1.670(4)
W2–O1	×2	2.295(4)	2.297(3)	–O10		1.632(5)	1.632(5)
–O2	×2	2.438(4)	2.428(3)		Mean	1.643	1.643
–O6		2.835(5)	2.819(4)				
–O9		2.480(5)	2.489(4)	Z3–O3	×2	1.629(3)	1.625(3)
–O10		2.426(5)	2.423(4)	–O6		1.630(5)	1.647(4)
	Mean	2.458	2.454	–O9		1.664(5)	1.646(4)
					Mean	1.638	1.636
X–O2	×2	2.102(3)	2.114(3)	Y–O1		1.983(3)	1.968(3)
–O9	×2	2.079(3)	2.076(3)	–O3		1.985(3)	1.967(3)
–O11	×2	1.972(3)	1.976(3)	–O4		2.099(3)	2.083(3)
	Mean	2.051	2.056	–O5		1.975(3)	1.968(3)
$V^{(VI)}$ (Å^3)		11.39	11.48	–O6		2.031(3)	2.013(3)
DI (oct)		0.026	0.026	–O7		1.966(3)	1.961(3)
<λ oct>		1.007	1.006		Mean	2.007	1.993
σ_θ (oct)^2		19.51	17.02	$V^{(VI)}$ (Å^3)		10.64	10.43
				DI (oct)		0.019	0.018
O5···O1**			2.876(5)	<λ oct>		1.008	1.009
O5···O5**			2.904(6)	σ_θ (oct)^2		25.72	27.39
O10···O5**		2.756(7)	2.750(6)				
O11···O7**		2.992(8)	2.962(6)	Si1–O8–Si2		131.7(3)	131.3(3)

* $DI(\text{oct}) = 1/6\Sigma|R_i - R_{av.}|/R_{av.}$ (R_i, each bond length; $R_{av.}$, average distance for an octahedron) (Baur, 1974), $\langle\lambda_{oct}\rangle = \sum_{i=1}^{6}(l_i - l_0)^2/6$ (l_i, each bond length; l_0, center-to-vertex distance for an octahedron with O_h symmetry, whose volume is equal to that of a distorted octahedron with bond lengths l_i) (Robinson et al., 1971), and $\sigma_\theta(\text{oct})^2 = \sum_{i=1}^{12}(\theta_i - 90^\circ)^2/11$ (θ_i, O-*M*-O angle) (Robinson et al., 1971).

** D···A oxygen donor-acceptor distances.

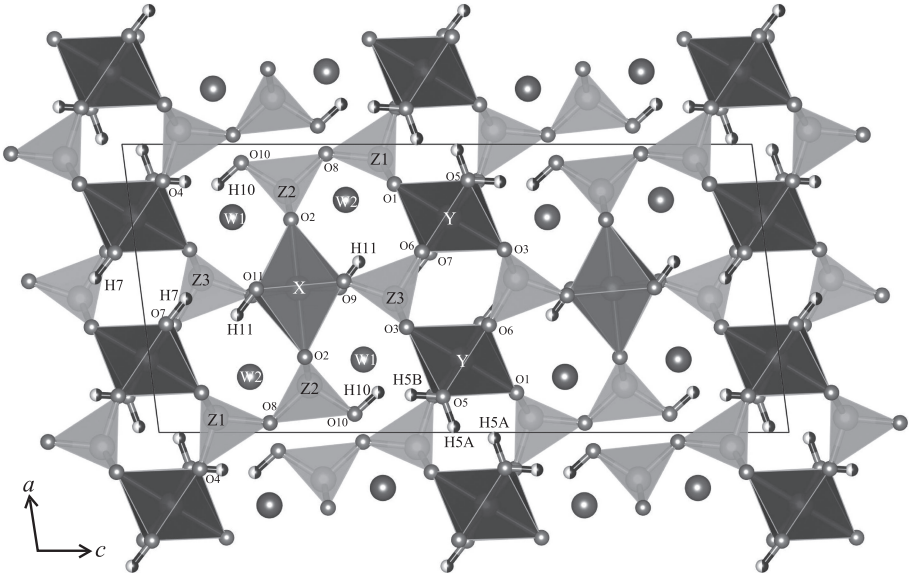

Figure 1. Crystal structure of poppiite projected along [010] drawn with VESTA3 (Momma and Izumi, 2011). The H5A site was not found in Komatsu poppiite.

determined site occupancies of Komatsu poppiite is $Ca_{2.00}{}^{X}(V^{3+}_{0.54}Fe^{3+}_{0.01}Mg_{0.19}Mn^{2+}_{0.22}Al_{0.04})^{Y}(V^{3+}_{1.73}Fe^{3+}_{0.03}Al_{0.24})Si_{3.00}O_{10.59}(OH)_{3.41}$ (Table 8). The number of hydroxyl group is estimated by the requirement of charge balance. The Nos. e^- of X and 2Y are 20.98 and 43.69, respectively. The Gambatesa poppiite is represented as $Ca_{2.00}{}^{X}(V^{3+}_{0.49}Fe^{3+}_{0.08}Mg_{0.19}Mn^{2+}_{0.17}Al_{0.07})^{Y}(V^{3+}_{1.35}Fe^{3+}_{0.21}Al_{0.44})Si_{3.00}O_{10.64}(OH)_{3.36}$ (Nos. e^- = 20.79 for X and 42.23 for 2Y) (Table 8). Both specimens analyzed by us are classified as poppiite-(V^{3+}). For pumpellyite, the Me^{2+}:Me^{3+} ratio var-

Table 6. Calculated ECoN(*ij*) for cation sites

	W1	W2	X	Y	Z1	Z2	Z3
Komatsu	6.78	6.15	5.83	5.90	3.98	3.99	3.99
Gambatesa	6.85	6.18	5.82	5.91	3.97	3.99	3.99

Table 7. Results of CD analyses

Cation		Komatsu	Gambatesa	Anion		Komatsu	Gambatesa
W1	$q(i)$	2.00	2.00	O1	$q(r)$	-2.00	-2.00
	$Q(ij)$	2.04	2.05		$Q(rs)$	-2.01	-2.02
	$q(ij)/Q(ij)$	0.98	0.98		$q(r)/Q(rs)$	1.00	0.99
W2	$q(i)$	2.00	2.00	O2	$q(r)$	-2.00	-2.00
	$Q(ij)$	2.02	2.02		$Q(rs)$	-1.97	-1.97
	$q(ij)/Q(ij)$	0.99	0.99		$q(r)/Q(rs)$	1.02	1.02
X	$q(i)$	2.85	2.76	O3	$q(r)$	-2.00	-2.00
	$Q(ij)$	2.83	2.74		$Q(rs)$	-1.89	-1.89
	$q(ij)/Q(ij)$	1.01	1.01		$q(r)/Q(rs)$	1.06	1.06
Y	$q(i)$	3.00	3.00	O4	$q(r)$	-2.00	-2.00
	$Q(ij)$	3.34	3.17		$Q(rs)$	-2.01	-1.98
	$q(ij)/Q(ij)$	0.90	0.95		$q(r)/Q(rs)$	1.00	1.01
Z1	$q(i)$	4.00	4.00	O5	$q(r)$	-2.00	-2.00
	$Q(ij)$	3.99	4.00		$Q(rs)$	-1.52	-2.05
	$q(ij)/Q(ij)$	1.00	1.00		$q(r)/Q(rs)$	1.32	0.98
Z2	$q(i)$	4.00	4.00	O6	$q(r)$	-2.00	-2.00
	$Q(ij)$	4.09	4.11		$Q(rs)$	-2.01	-1.95
	$q(ij)/Q(ij)$	0.98	0.97		$q(r)/Q(rs)$	1.00	1.03
Z3	$q(i)$	4.00	4.00	O7	$q(r)$	-2.00	-2.00
	$Q(ij)$	4.10	4.10		$Q(rs)$	-1.60	-1.60
	$q(ij)/Q(ij)$	0.98	0.98		$q(r)/Q(rs)$	1.25	1.25
H5A	$q(i)$	-	0.50	O8	$q(r)$	-2.00	-2.00
	$Q(ij)$	-	0.49		$Q(rs)$	-1.99	-1.99
	$q(ij)/Q(ij)$	-	1.02		$q(r)/Q(rs)$	1.01	1.01
H5B	$q(i)$	0.50	0.50	O9	$q(r)$	-2.00	-2.00
	$Q(ij)$	0.63	0.50		$Q(rs)$	-2.03	-2.07
	$q(ij)/Q(ij)$	0.79	1.00		$q(r)/Q(rs)$	0.99	0.97
H7	$q(i)$	0.50	0.50	O10	$q(r)$	-2.00	-2.00
	$Q(ij)$	0.61	0.63		$Q(rs)$	-1.91	-1.86
	$q(ij)/Q(ij)$	0.82	0.79		$q(r)/Q(rs)$	1.05	1.08
H10	$q(i)$	0.50	0.50	O11	$q(r)$	-2.00	-2.00
	$Q(ij)$	0.54	0.53		$Q(rs)$	-2.05	-1.99
	$q(ij)/Q(ij)$	0.93	0.94		$q(r)/Q(rs)$	0.98	1.01
H11	$q(i)$	0.50	0.50		σ (%)	4.9	3.8
	$Q(ij)$	0.50	0.50				
	$q(ij)/Q(ij)$	1.00	1.00				
	σ (%)	7.1	4.2				

Table 8. Determined site occupancies of poppiite crystals*

	X	Y
Komatsu	$V^{3+}_{0.54}Fe^{3+}_{0.01}Mg_{0.19}Mn^{2+}_{0.22}Al_{0.04}$	$V^{3+}_{0.865}Fe^{3+}_{0.017}Al_{0.118}$
Gamabatesa	$V^{3+}_{0.49}Fe^{3+}_{0.08}Mg_{0.19}Mn^{2+}_{0.17}Al_{0.07}$	$V^{3+}_{0.676}Fe^{3+}_{0.104}Al_{0.220}$

* The cation contents are fixed by EMPA data.

ies at the X site between 0.4:0.6 and 0.6:0.4, in general (e.g., Passaglia and Gottardi, 1973; Deer et al., 1986). In this study, the corresponding ratio at X in this study is 0.41: 0.59 for the Komatsu specimen, and 0.36:0.64 for the Gambatesa one. Both specimens tend to have high Me^{3+}.

Structural variations of poppiite

The positive correlation between <Y-O> and the mean ionic radius at Y proposed in several previous studies is also confirmed (R^2 = 0.932 in Fig. 2). In Figure 3, the average ionic radius at the Y site is plotted versus the unit-cell parameters for a set of pumpellyite-group minerals, including poppiite (V^{3+}-analogue) and julgoldite. Because of low quality of cell-dimension data, values for shuiskite (Ivanov et al., 1981) and okhotskite (Togari and Akasaka, 1987; Akasaka et al., 1997) are not shown. The unit-cell volume of the Komatsu poppiite (1033.2 Å^3) is obviously larger than that of the Gambatesa one (1026.6 Å^3 in this study; 1026.7 Å^3 in Brigatti et al., 2006) (Fig. 3e) due to the high V content in the Komatsu sample. It has been known that the unit-cell parameters of pumpellyite-group minerals strongly depend on the mean ionic radius at the Y site (Fig. 3) while there is

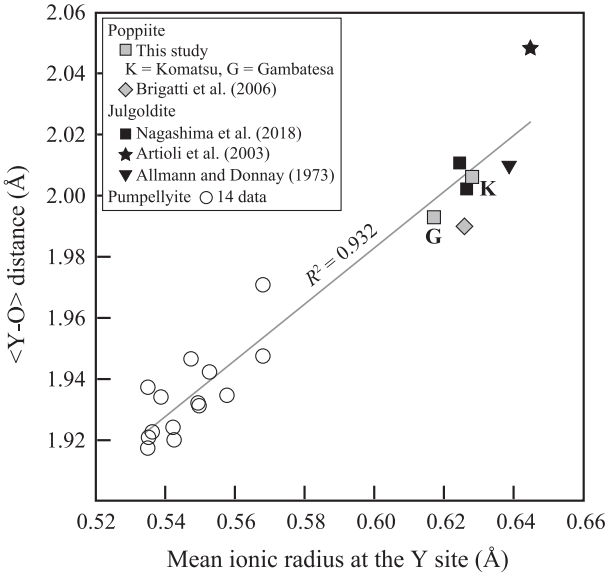

Figure 2. The <Y-O> distance (Å) versus the mean ionic radius (Å) at the Y site. The symbols are significantly larger than the associated standard deviations. Data sources of the 14 pumpellyite specimens plotted in this figure are as follows; Artioli and Geiger (1994), Hamada et al. (2010), Hatert et al. (2007); Nagashima et al. (2006, 2010) and Yoshiasa and Matsumoto (1985).

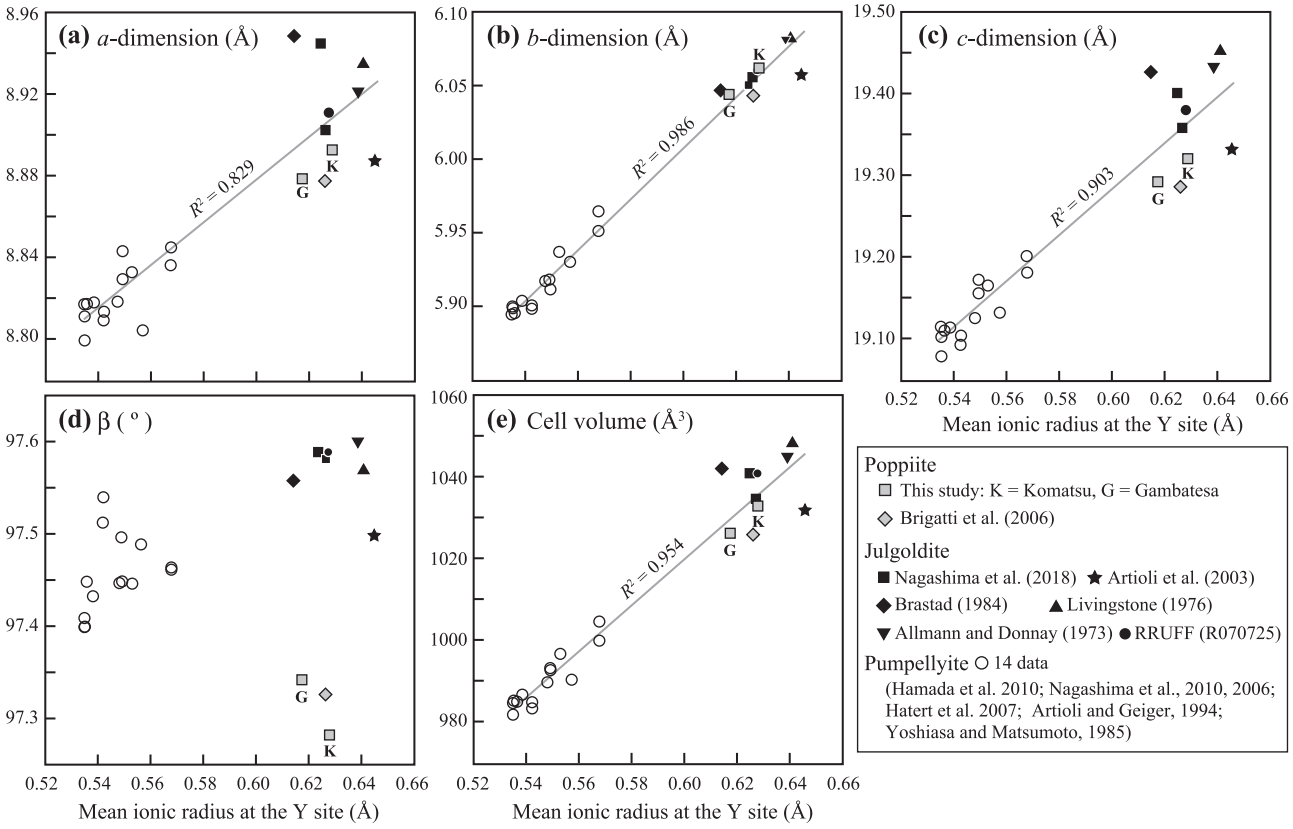

Figure 3. Cell-dimension data of pumpellyite-group minerals plotted versus the mean ionic radius (Å) at the Y site. The symbols are significantly larger than the associated standard deviations.

Table 9. Determined H atomic positions in pumpellyite-group minerals

Mineral name	Sample name or locality	H atomic positions						References
		H5A	H5B	H7A	H7B	H10	H11	
Poppiite-(V^{3+})	Komatsu		O		O	O	O	This study
	Gambatesa	O	O		O	O	O	
	Gambatesa	O		O		O	O	Brigatti et al. (2006)
Julgoldite-(Fe^{2+})	Bombay	O		O		O	O	Nagashima et al. (2018)
	Kreimbach/Kaulbach	O		O	O	O	O	
Pumpellyite-(Mg)	OHS	O	O	O		O	O	Nagashima et al. (2010)
	SAR	O	O	O		O	O	
	Sarany	O		O		O	O	Nagashima et al. (2010)
	ocp1211			O		O	O	Hamada et al. (2010)
	ocp0604	O		O				
	ocp1016					O		
Pumpellyite-(Al)	ocp1028			O			O	Hamada et al. (2010)
	Oonara	O		O		O	O	Yoshiasa and Matsumoto (1985)

no correlation between the mean radius of the X site occupants and the <X-O> distance or the volume (Nagashima et al., 2006; Nagashima and Akasaka, 2007). Recently Nagashima et al. (2018) proposed that the variation of the ***b***-dimension is governed by the smaller octahedra, XO_6 or YO_6. In the present study, the mean ionic radius at Y is smaller than that at X in both poppiite specimens, suggesting that the variation of ***b***-dimension is governed by the size of YO_6 (Fig. 3b). Furthermore, the variation of ***a***- and ***c***-dimensions are explained by the lateral extension of the (010) plane, which acts as buffer to compensate for the larger XO_6 octahedra (Nagashima et al., 2018). If $Me^{2+}/Me^{3+} > 1$ at X, the ***a***- and ***c***-dimensions are increased compared to the expected values from the regression lines estimated for an approximate Me^{2+}:Me^{3+} = 0.5:0.5. In contrast, the short ***a***- and ***c***-dimensions imply the high proportion of Me^{3+} at X. The ***a***- and ***c***-dimensions of poppiite in this study are shorter than those values predicted by regression lines (Figs. 3a and 3c), suggesting that X is predominantly occupied by Me^{3+}. This is consistent with the determined site occupancies at X in poppiites (Me^{2+}:Me^{3+} = 0.41:0.59 for the Komatsu specimen, and 0.36:0.64 for the Gambatesa one).

Poppiite is characterized by a small β angle, 97.283(2)° for Komatsu, 97.343(3)° for Gambatesa (this study), and 97.328(2)° for Gambatesa by Brigatti et al. (2006) (Fig. 3d) compared to other pumpellyite-group minerals. This deviation is probably related to varying distortions of YO_6 octahedra caused by the different characteristics of octahedral V^{3+} ions compared to Fe^{3+} and Cr^{3+}.

Hydrogen bond system in pumpellyite

Based on the determined H atomic positions in single-crystal structural studies listed in Table 9, the possible H atom positions in the pumpellyite structure can be summarized as H5A, H5B, H7A, H7B, H10, and H11 (Fig. 4). All donor oxygen-hydrogen bonds of pumpellyite group minerals are located on mirror planes parallel to (010) as suggested by Yoshiasa and Matsumoto (1985). The relationship between donor and acceptor oxygen atoms and their hydrogen bonds in our studied crystal can be summarized as follows: (1) bifurcated O5-H5A···O1/O5-H5A···O5, (2) O5-H5B···O10, (3) bifurcated O7-H7A···O3/O7-H7A···O7, (4) O7-H7B···O11, (5) O10-H10···O5, and (6) O11-H11···O7 (Fig. 4, Table 10). As the results of CD methods (Table 7), the $Q(rs)$ values of O5 (−1.52) and O7 (−1.60) significantly deviate from the expected value (−2.00) for the Komatsu poppiite. This may indicate the presence of undetermined H sites attached to O5 and O7. The deviation of $Q(rs)$ from the expected value was also observed for O7 (−1.60) in the Gambatesa poppiite with H7B assumed to be half occupied.

Yoshiasa and Matsumoto (1985) suggested that the Me^{2+} or Me^{3+} distribution at X is counterbalanced by a number of hydroxyl groups as the result of following substitution mechanism: $Me^{3+} + 3OH^- + O^{2-} \leftrightarrow Me^{2+} + 4OH^-$. The combination of H atoms leads to the five possible hydrogen-bond systems (a)-(e) including 2-4 hydroxyls (Table 10). All possible combinations may be present in the pumpellyite structure. However, the hydrogen-bond system (e) having only 2 OH groups must be uncommon because the 3-4 hydroxyls are required to maintain the local charge balance.

Pumpellyite, sursassite and macfallite structures have one Si-OH unit in common, the so-called silanol group. The Z2-O10 bond in pumpellyite represents a silanol group, which is topologically similar to Si3-O10 in iso-structural macfallite and sursassite. It is known that

Table 10. Possible hydrogen-bond systems in pumpellyite, and the similar H positions in structurally related minerals, macfallite and sursassite

	Number of OH	O5-H5A⋯ O1/O5	O5-H5B⋯ O10	O7-H7A⋯ O3/O7	O7-H7B⋯ O11	O10-H10⋯O5	O11-H11⋯O7
Pumpellyite (a)	4	O		O		O	O
(b)	3		O	O			O
(c)	3	O			O	O	
(d)	3		O	O			O
(e)	2		O		O		
Macfallite*		O (H6)	O (H11)	O (H6)	O (H11)	O (H10)	
Sursassite**		O (H6B, H11A)	O (H6A)	O (H6B, H11A)	O (H11B)	O (H10)	O (H7)

Note: The original site names of macfallite and sursassite are written in parentheses.
* Nagashima et al. (2008). ** Nagashima et al. (2009).

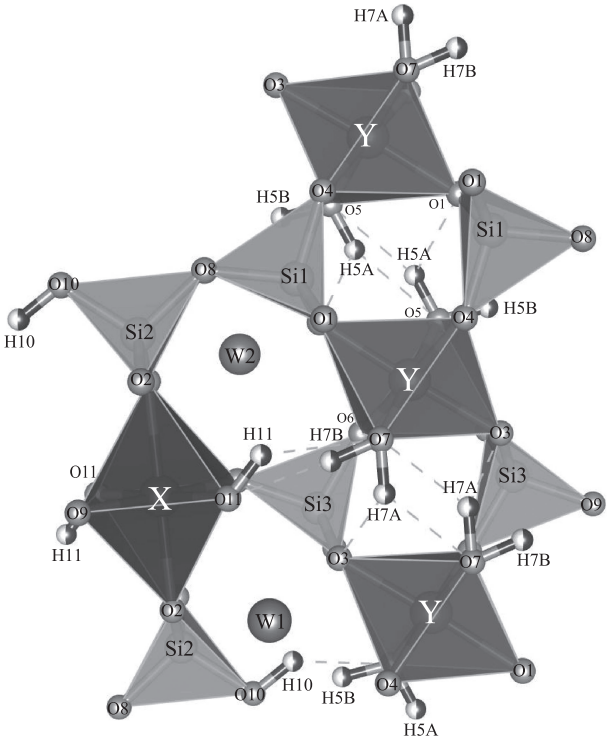

Figure 4. Hydrogen-bond system in pumpellyite projected down [010].

the protonation of one tetrahedral apex allows variations in Si-O bond lengths and distorts the tetrahedron (Nyfeler and Armbruster, 1998). In macfallite, O10 represents a fully occupied silanol group with lengthened Si3-O10 bond (Nagashima et al. 2008), as predicted by Nyfeler and Armbruster (1998). This lengthening is not observed in pumpellyite and sursassite. In contract, the Z2-O10 bond in poppiite is the shortest one within the Z2 tetrahedron (Table 5). In most other structural studies of pumpellyite-group minerals, the Z2-O10 bond tends to be shorter than average. In addition, the corresponding Si3-O10 bond in sursassite is also the shortest bond within the Si3 tetrahedron (Nagashima et al., 2009). Thus, a complete silanol group at O10 in both minerals can be excluded. The short Z2-O10 distance in the pumpellyite structure suggests vacancies at H10.

ACKNOWLEDGMENTS

We thank the Editor Prof. N. Shimobayashi, as well as two anonymous reviewers for their constructive comments. We also thank Prof. M. Akasaka and Dr. M. Tasaka for their permission to use Bruker SMART APEXII at Shimane University, Mr. Y. Maki (Rigaku Corporation) for his arrangement to use RIGAKU HyPix-6000HE, Mr. Y. Morifuku for his technical assistance in using EMPA, and Prof. T. Armbruster for his constructive comment on this manuscript. One of the authors (M.N.) gratefully acknowledges the financial supports of Grant-in-Aid for Scientific Research from the Japan Society for the Promotion of Science, nos. JP25800296 and JP18K03782.

REFERENCES

Akasaka, M., Kimura, Y., Omori, Y., Sakakibara, M., Shinno, I. and Togari, K. (1997) ^{57}Fe Mossbauer study of pumpellyite-okhotskite-julgoldite series minerals. Mineralogy and Petrology, 61, 181-198.

Allmann, R. and Donnay, G. (1971) Structural relations between pumpellyite and ardennite. Acta Crystallographica, B27, 1871-1875.

Allmann, R. and Donnay, G. (1973) The crystal structure of julgoldite. Mineralogical Magazine, 39, 371-281.

Artioli, G. and Geiger, C.A. (1994) The crystal chemistry of pumpellyite: An X-ray Rietveld refinement and ^{57}Fe Mössbauer study. Physics and Chemistry of Minerals, 20, 443-453.

Artioli, G., Geiger, C.A. and Dapiaggi, M. (2003) The crystal chemistry of julgoldite-Fe^{3+} from Bombay, India, studied us-

ing synchrotron X-ray powder diffraction and ^{57}Fe Mössbauer spectroscopy. American Mineralogist, 88, 1084-1090.

Baur, H. (1974) The geometry of polyhedral distortions. Predictive relationships for the phosphate group. Acta Crystallographica, B30, 1195-1215.

Brastad, K. (1984) Julgoldite from Tafjord, Sunnmøre. Contribution to the Mineralogy of Norway, No. 67. Norsk geologisk tidsskrift, 3, 251-255.

Brigatti, M.F., Caprilli, E. and Marchesini, M. (2006) Poppiite, the V^{3+} end-member of the pumpellyite group: Description and crystal structure. American Mineralogist, 91, 584-588.

Bruker (1999) SMART and SAINT-Plus. Versions 6.01. Bruker AXS Inc., Madison, Wisconsin, USA.

Deer, W.A., Howie, R.A. and Zussman, J. (1986) Rock-forming minerals. 1B (Second edition), Disilicates and ring silicates. pp. 629, Geological Society Publishing House, UK.

Franks, F. (1973) Water: A comprehensive treatise. vol. 2, Water in Crystalline Hydrates Aqueous Solutions of Simple Nonelectrolytes. pp. 684, Plenum, New York.

Gottardi, G. (1965) Die Kristallstruktur von Pumpellyit. Tschermaks mineralogische und petrographische Mitteilungen, 10, 115-119 (in German).

Hamada, M., Seto (Sakamoto), S., Akasaka, M. and Makino, K. (2010) Crystal chemistry of chromian pumpellyite from Osayama, Okayama Prefecture, Japan. American Mineralogist, 95, 1294-1304.

Hatert, F., Pasero, M., Perchiazzi, N. and Theye, T. (2007) Pumpellyite-(Al), a new mineral from Bertrix, Belgian Ardennes. European Journal of Mineralogy, 19, 247-253.

Hoppe, R. (1979) Effective coordination numbers (ECoN) and mean fictive ionic radii (MEFIR). Zeitschirift für Kristallographie, 150, 23-52.

Ivanov, O.K., Arkhangel'skaya, V.A., Miroshnikova, L.O. and Shilova, T.A. (1981) Shuiskite, the chromium analogue of pumpellyite, from the Bisersk deposit, Urals. Zapiski Vsesojuznogo mineralogischeskogo Obshchestva, 110, 508-512 (in Russian).

Livingstone, A. (1976) Julgoldite, new data and occurrences; a second recording. Mineralogical Magazine, 40, 761-763.

Momma, K. and Izumi, F. (2011) VESTA 3 for three-dimensional visualization of crystal, volumetric and morphology data. Journal of Applied Crystallography, 44, 1272-1276.

Nagashima, M., Ishida, T. and Akasaka, M. (2006) Distribution of Fe among octahedral sites and its effect on the crystal structure of pumpellyite. Physics and Chemistry of Minerals, 33, 178-191.

Nagashima, M. and Akasaka, M. (2007) The distribution of chromium in chromian pumpellyite from Sarani, Urals, Russia: a TOF neutron and X-ray Rietveld study. Canadian Mineralogist, 45, 837-846.

Nagashima, M., Rahmoun, N.-S., Alekseev, E.V., Geiger, C.A., Armbruster, T. and Akasaka, M. (2008) Crystal chemistry of macfallite: Relationships to sursassite and pumpellyite. American Mineralogist, 70, 171-181.

Nagashima, M., Akasaka, M., Minakawa, T., Libowitzky, E. and Armbruster, T. (2009) Sursassite: Hydrogen bonding, cation order, and pumpellyite intergrowth. American Mineralogist, 94, 1440-1449.

Nagashima, M., Armbruster, T. and Libowitzky, E. (2010) The hydrogen-bond system in pumpellyite. European Journal of Mineralogy, 22, 333-342.

Nagashima, M., Cametti, G. and Armbruster, T. (2018) Crystal chemistry of julgoldite, a mineral series of the pumpellyite group: Re-investigation of Fe distribution and hydrogen-bonding. European Journal of Mineralogy, 30, 721-731.

Nespolo, M. (2016) Charge distribution as a tool to investigate structural details. IV. A new route to heteroligand polyhedra. Acta Crystallographica, B72, 51-66.

Nespolo, M., Ferraris, G. and Ohashi, H. (1999) Charge distribution as a tool to investigate structural details: meaning and application to pyroxenes. Acta Crystallographica, B55, 902-916.

Nespolo, M., Ferraris, G., Ivaldi, G. and Hoppe, R. (2001) Charge distribution as a tool to investigate structural details. II. Extension to hydrogen bonds, distorted and hetero-ligand polyhedra. Acta Crystallographica, B57, 652-664.

Nyfeler, D. and Armbruster, T. (1998) Silanol groups in minerals and inorganic compounds. American Mineralogist, 83, 119-125.

Pan, Y. and Fleet, M.E. (1992a) Mineral chemistry and geochemistry of vanadian silicates in the Hemlo gold deposit, Ontario, Canada. Contributions to Mineralogy and Petrology, 109, 511-525.

Pan, Y. and Fleet, M.E. (1992b) Vanadium-rich minerals of the pumpellyite group from the Hemlo gold deposit, Ontario. Canadian Mineralogist, 30, 153-162.

Passaglia, E. and Gottardi, G. (1973) Crystal chemistry and nomenclature of pumpellyites and julgoldites. Canadian Mineralogist, 12, 219-223.

Rigaku Oxford Diffraction (2018) CrysAlisPro Software system, version 1.171.39.45e, Rigaku Corporation, Oxford, UK.

Robinson, K., Gibbs, G.V. and Ribbe, P.H. (1971) Quadratic elongation: a quantitative measure of distortion in coordination polyhedra. Science, 172, 567-570.

Shannon, R.D. (1976) Revised effective ionic radii and systematic studies of interatomic distances in halides and chalcogenides. Acta Crystallographica, A32, 751-767.

Sheldrick, G.M. (1996) SADABS. University of Göttingen, Germany.

Sheldrick, G.M. (2008) A short history of SHELX. Acta Crystallographica, A64, 112-122

Togari, K. and Akasaka, M. (1987) Okhotskite, a new mineral, an Mn^{3+}-dominant member of the pumpellyite group, from the Kokuriki mine, Hokkaido, Japan. Mineralogical Magazine, 51, 611-614.

Yamada, T. and Takizawa, M. (2007) Vanadium-bearing minerals from the Komatsu mine, Saitama Prefecture. Abstracts with Program 2007 Annual Meeting of Japan Association of Mineralogical Sciences, 199, K8-03 (in Japanese with English Abstract).

Yamada, T., Momma, K., Miyawaki, R., Matsubara, S., Ishibashi, T., Fujiwara, T. and Takizawa, M. (2014) A vanadium-rich pumpellyite group mineral from the Komatsu mine, Saitama Prefecture, Japan. Abstracts with Program 2014 Annual Meeting of Japan Association of Mineralogical Sciences, 55, R1-P12 (in Japanese with English Abstract).

Yoshiasa, A. and Matsumoto, T. (1985) Crystal structure refinement and crystal chemistry of pumpellyite. American Mineralogist, 70, 1011-1019.

Manuscript received June 13, 2018
Manuscript accepted September 11, 2018

Manuscript handled by Norimasa Shimobayashi